The phase transition and elastic and optical properties of polymorphs of CuI

The phase transition and elastic and optical properties of polymorphs of CuI

Jiajie Zhu[1,3], Ravindra Pandey[1] and Mu Gu[2]

[1] Department of Physics, Michigan Technological University, Houghton, MI 49931, USA
[2] Department of Physics, Tongji University, Shanghai 200092, People's Republic of China

E-mail: pandey@mtu.edu

Abstract
The high-pressure polymorphs of CuI have attracted much attention due to the somewhat contradictory identification of their structures by means of x-ray diffraction measurements and theoretical calculations. In this paper, we report the results of a theoretical investigation of polymorphs of CuI including zinc-blende, rhombohedral, tetragonal, rocksalt and orthorhombic phases. We find that CuI follows the high-pressure transition path from the zinc-blende phase to the orthorhombic phase via the tetragonal phase, and the rhombohedral phase shows mechanical instability under high pressure. The bulk moduli are almost isotropic but the shear moduli show large anisotropy in these polymorphs. A relatively strong hybridization of I p and Cu d states appears to determine the electronic properties of the CuI polymorphs. The zinc-blende and tetragonal CuI are direct gap semiconductors and their optical properties are similar, whereas the orthorhombic CuI is metallic.

S Online supplementary data available from stacks.iop.org/JPhysCM/24/475503/mmedia

(Some figures may appear in colour only in the online journal)

1. Introduction

Cuprous iodine (CuI) is a well-known optical material with many interesting physical and chemical properties such as high ionic conductivity ($\approx$0.1 S cm^{-1}), wide band gap ($\approx$3.1 eV), and large excitonic binding energy ($\approx$62 meV) [1–4]. It has also attracted much attention as an ultrafast scintillator due to its fast decay time of about 130 ps [5, 6]. At ambient conditions, CuI occurs in the zinc-blende (γ) phase, though it can be transformed into several polymorphs at high temperature and high pressure. At ambient pressure, a high-temperature phase transition from the zinc-blende (γ) phase to the hexagonal (β) phase between 642 and 680 K, and the cubic (α) phase above 680 K is reported [7]. The successive high-pressure polymorphs of CuI, on the other hand, are reported to be rhombohedral (<1.4 GPa), tetragonal (1.4–4.7 GPa) and rocksalt (>10 GPa) phases by the experimental studies [8–10]. Surprisingly, theoretical calculations based on

density functional theory do not find the high-pressure phase transition from zinc-blende to rhombohedral [11–14]. This is in spite of the fact that first-principles calculations with proven predictive capabilities are now routinely performed on a wide variety of materials to gain an understanding of their structural, thermodynamic, electronic and optical properties [15]. Furthermore, experimental and theoretical investigations have so far only focused on determining a limited set of structural and electronic properties of polymorphs of CuI. These properties include lattice constants, bulk modulus and electronic band structures of polymorphs of CuI. And to the best of our knowledge, a detailed study of elastic and optical properties of these polymorphs including the orthorhombic phase of CuI has not been performed previously.

In this paper, we will perform a comprehensive theoretical study of polymorphs of CuI. Specifically, we will focus on calculations of elastic constants to examine the stability of the high-pressure rhombohedral phase. Our results will suggest that the rhombohedral phase is not stable, and the phase transition from tetragonal to

[3] Permanent Address: Department of Physics, Tongji University, Shanghai, People's Republic of China.

orthorhombic via rocksalt is not preferred. We will also calculate the electronic properties including effective electron mass, optical reflectivity, index of refraction and optical absorption coefficients of the high-pressure polymorphs of CuI.

In section 2, we describe the computational method. In section 3, we present the results and discussion and give a brief summary in section 4.

2. Computational method

The electronic structure calculations are carried out using the projector augmented plane-wave (PAW) method as implemented in Vienna *ab initio* simulation package (VASP) [16, 17]. The generalized gradient approximation (GGA) of Perdew, Burke and Ernzerhof (PBE) is adopted for the exchange–correlation potential [18] to the density functional theory (DFT). The 3d and 4s electrons of Cu together with 5s and 5p electrons of I are considered as the valance electrons in the calculations.

The Brillouin-zone integrations are performed with the $10 \times 10 \times 10$ k-point mesh for the structural optimization calculations. Later, a $16 \times 16 \times 16$ k-point mesh is used for density of state (DOS) calculations. The cut-off energy for plane-wave basis is 355 eV. The energy tolerance is 10^{-6} eV in the iterative solution of the Kohn–Sham equations. The structure and atoms are relaxed until the force on each atom is less than 0.01 eV Å^{-1}. For a larger plane-wave cut-off value of 500 eV with a denser k-point mesh of $20 \times 20 \times 20$, the change in total energy is about 0.02 eV/atom. A similar variation is predicted for the exchange–correlation functional form at the GGA-DFT level of theory. Thus, the residual numerical uncertainty is estimated to be about 0.04 eV/atom in our calculations.

The elastic constants are determined using second-order derivatives of equilibrium energy with respect to strains via

$$C_{\alpha\beta} = \frac{1}{V} \frac{\partial^2 E}{\partial \gamma_\alpha \partial \gamma_\beta}, \qquad (1)$$

where γs are applied strains in Voigt's notion around the equilibrium position [19]. The deformations of polymorphs of CuI depend on their space groups.

The imaginary part of dielectric function, $\varepsilon_2(\omega)$, is determined by the summation over occupied states in the valence band and unoccupied states in the conduction band using the equation:

$$\varepsilon_2^{\alpha\beta}(\omega) = \frac{4\pi^2 e^2}{V} \lim_{q \to 0} \frac{1}{q^2} \sum_{c,v,k} 2\omega_k \delta(\epsilon_{ck} - \epsilon_{vk} - \omega)$$
$$\times \langle u_{ck+e_\alpha q} \mid u_{vk} \rangle \langle u_{ck+e_\beta q} \mid u_{vk} \rangle^* \qquad (2)$$

where the index v and c refer to the valence band and conduction band and u_{ck} is the cell periodic part of wave function at different k-point [20]. The real part of dielectric function is obtained from Kramers–Kronig transformation via

$$\varepsilon_1(\omega) = 1 + \frac{2}{\pi} \int_0^\infty \frac{\omega' \varepsilon_2(\omega') \mathrm{d}\omega'}{(\omega'^2 - \omega^2)}. \qquad (3)$$
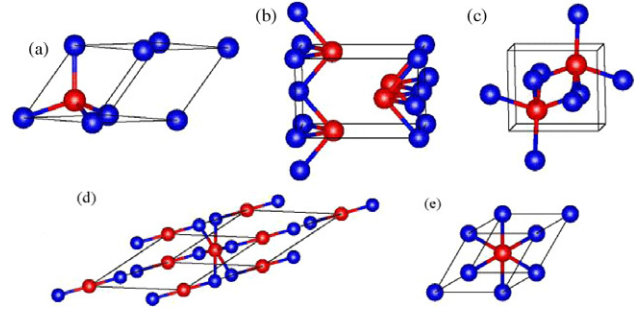

Figure 1. A schematic diagram of polymorphs of CuI: (a) zinc-blende, (b) tetragonal, (c) orthorhombic, (d) rhombohedral and (e) rocksalt.
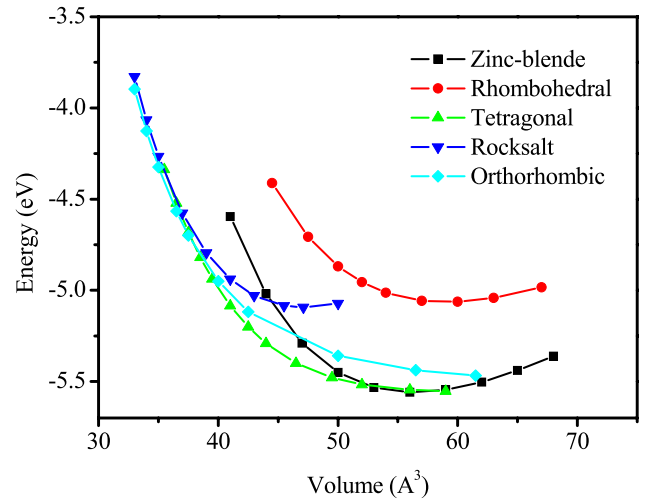

Figure 2. Total energy/formula unit as a function of volume for polymorphs of CuI.

The refractive index is calculated by

$$n(\omega) = \left(\frac{\sqrt{\varepsilon_1^2(\omega) + \varepsilon_2^2(\omega)} + \varepsilon_1(\omega)}{2} \right)^2. \qquad (4)$$

3. Results and discussion

3.1. Structural properties

The crystal structures of the polymorphs of CuI are illustrated in figure 1. The calculated energy surface of these structures is given in figure 2 where the total energy of per CuI formula unit is plotted as a function of the crystallographic unit-cell volume of the several polymorphs of CuI. The lattice parameters as well as the internal coordinates are optimized at each fixed value of unit-cell volume. The zinc-blende phase is predicted to be the most stable phase as also experimentally observed. It is followed by the tetragonal phase with a noticeable contracted equilibrium volume ($\approx 10\%$) and the energy difference of about 0.06 eV.

It is generally understood that a common-tangent construction for the energy versus volume curves of two

Table 1. The calculated structural properties of polymorphs of CuI at the GGA-DFT level of theory.

	Space group	Lattice constant (Å)		Volume/unit cell (Å³)	Cohesive energy (eV)	Bond distance R (Cu–I) (Å)
		This work	Expt [8, 22]	This work	This work	This work
Zinc-blende	216	$a = 6.074$	$a = 6.054$	56.0	5.56	2.63
Rhombohedral	166	$a = 4.452$	$a = 4.155$	58.6	5.06	2.72
		$c = 20.49$	$c = 20.48$			
Tetragonal	129	$a = 4.063$	$a = 4.023$	50.6	5.5	2.65
		$c = 6.206$	$c = 5.651$			
Rocksalt	225	$a = 5.733$		47.1	5.09	2.87
Orthorhombic	63	$a = 5.419$	$a = 5.373$	37.5	4.69	2.53
		$b = 6.168$	$b = 6.115$			
		$c = 4.495$	$c = 4.609$			

phases of a system yields the high-pressure transitional pressure. Following this guideline, figure 2 suggests that there exists no phase transition between the zinc-blende and the rhombohedral phase of CuI. The energy difference between these two phases is calculated to be about 0.5 eV. Likewise, calculations suggest that there appears to be a phase transition from the zinc-blende phase to the rocksalt phase, though a possibility of the phase transition from the rocksalt phase to either the tetragonal phase or the orthorhombic phase does not exist in CuI.

The structural parameters including lattice constants together with equilibrium volumes and cohesive energies of CuI in its ambient and high pressure polymorphs are presented in table 1. We find that the calculated structural properties of the well-characterized zinc-blende phase are in excellent agreement with the previously reported experimental and theoretical values suggesting the accuracy and reliability of our modeling parameters. For example, the equilibrium volume of the zinc-blende phase is calculated to be 56 Å³. The corresponding experimental value is 55.5 Å³. For the high-pressure orthorhombic phase, the lattice constant values are 5.419, 6.168 and 4.495 Å, as compared to the corresponding experimental values of 5.373, 6.115 and 4.609 Å, respectively. The calculated internal coordinates of tetragonal and orthorhombic phases are (Cu: (0, 0, 0), I: (0, 0.5, 0.276)), and (Cu; (0, 0, 0), I: (0, 0.5, 0.276)), respectively. The structural parameters associated with the tetragonal and orthorhombic phases are calculated at 2.4 GPa and 19.6 GPa, respectively at which the phase transition from the zinc-blende phase is expected to occur.

The cohesive energy values given in table 1 suggest the predicted order of stability to be zinc-blende > tetragonal > rocksalt > rhombohedral > orthorhombic for CuI. The cohesive energy is defined as difference between the total energy of bulk CuI and the sum of total energies of Cu atom and I atom.

A change in the coordination number from four (zinc-blende) to five (orthorhombic) occurs with the pressure and is accompanied by the volume contraction of 33%. The near-neighbor distance R_{Cu-I} decreases from 2.63 Å for the zinc-blende phase to 2.53 Å for the orthorhombic phase. As expected, the nature of chemical bonding also changes in going from zinc-blende to tetragonal to orthorhombic as

evidenced by the projected electron localization functions (ELFs) in figure 3 [21]. The maximum value of ELF around Cu ion is about 0.77 in the orthorhombic CuI. Note that the values of ELF vary from 0 to 1, which represents complete delocalization and complete localization respectively.

3.2. Phase transition

The transition pressure is defined as the pressure where the enthalpy $H = E + PV$ of two phases are equal. The first phase transition, from zinc-blende to tetragonal, occurs at about 2.4 GPa. The volume contraction is about 10%, as indicated in figure 4. The second phase transition, from tetragonal to orthorhombic is observed at about 19.6 GPa and the corresponding volume contraction is 26%. The phase transition from the tetragonal phase to the orthorhombic phase does not occur via the rocksalt phase. Also, no phase transition from the orthorhombic phase to the rocksalt phase is seen up to 40 GPa.

Our theoretical results are in a very good agreement with the experimental results [22], though they do not agree with the results obtained by the atomistic calculations [23]. We believe that the use of the atomistic method which lacks the important exchange and correlation contributions may result in predicting the stability of the rocksalt phase between 10 and 18 GPa. Furthermore, our calculations find the total energy of the rocksalt and the orthorhombic phases to be almost degenerate at high pressures (figure 2) suggesting the phase transition to occur at high pressure and high temperature conditions.

A direct phase transition from the zinc-blende to the rocksalt phase at about 9.6 GPa is also predicted. This result is in agreement with the previously theoretical results [12–14]. Note that the phase transition from the zinc-blende phase to the rocksalt phase has been seen in CuCl and CuBr, though it occurs via intermediate phases less than 10 GPa [8].

3.3. Elastic properties

Table 2 lists the calculated elastic properties, including elastic constants, bulk and shear moduli and Debye temperature of polymorphs of CuI. For the well-characterized zinc-blende phase, the calculated elastic properties and Debye temperature
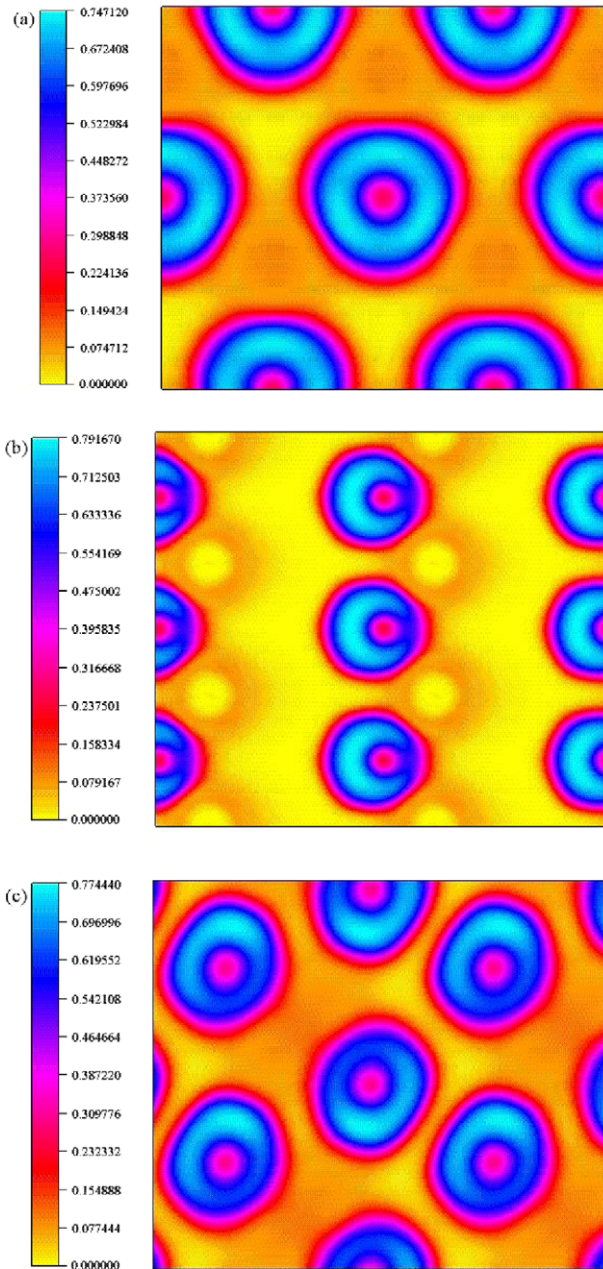
Figure 3. The projected electron localization functions of CuI: (a) Zinc-blende, (b) tetragonal and (c) orthorhombic.

Figure 4. A schematic diagram of the pressure–volume curve for CuI.

We use the subscripts V, R and H to donate Voigt, Reuss and Hill notation, where K_H (G_H) is the average value of K_V (G_V) and K_R (G_R). B_X is the bulk modulus along x-axis of a system under hydrostatic pressure. Since dispersion in the directional bulk moduli along different crystal axes reveals the anisotropy of the system, we define the percentage of anisotropy to be $(B_X - B_Z)/(B_X + B_Z) \times 100\%$ for x and z direction in the lattice. It is to be noted here that the predicted anisotropy is 18% for x and z direction in the tetragonal phase but 32% in the orthorhombic phase. This is due to the fact that CuI makes a transition from four-coordinated lattice structure to the five-coordinated lattice structure, leading to a strong dependence of lattice constants with pressure in the orthorhombic CuI (figure S1 available at stacks.iop.org/JPhysCM/24/475503/mmedia).

3.4. Electronic properties

The calculated density of states (DOS) and band structures are shown in figures 5 and 6, respectively. For the zinc-blende phase, the uppermost valence band is formed by Cu 3d and I 5p states, and the valence band maximum (VBM) is mainly composed of I 5p states with three-fold degeneracy. There is a relatively narrower I 5s band located at 13 eV below VBM. For the tetragonal CuI, I 5s band now splits into two sub-bands reducing its separation with the upper valence band. For zinc-blende, tetragonal and orthorhombic CuI, the conduction band minimum (CBM) is all composed of the Cu 4s states with a parabolic character.

The calculations find the zinc-blende to be a direct gap semiconductor with a gap of 1.13 eV. It is similar to the values obtained previously [12], though the experimental value is 3.1 eV. For the tetragonal phase, the calculated direct gap at Γ is 1.54 eV and the indirect (Γ–M) gap is 2.35 eV. The orthorhombic CuI shows metallic character due to the crossing of Cu 4s and I 5p states at the Fermi energy. Here, the Cu 3d band is pushed down to lower energy away from VBM. It should be pointed out that the GGA-DFT method underestimates the band gap of the semiconducting and ionic

are in excellent agreement with the corresponding experiment values [24, 25].

The elastic constants of orthorhombic structure are characterized by nine independent components, i.e. C_{11}, C_{12}, C_{13}, C_{22}, C_{23}, C_{33}, C_{44}, C_{55} and C_{66}. For tetragonal structure, the independent components reduce to six and they further decrease to three for the zinc-blende structure. K and G are average bulk and shear modulus, respectively [26]. Following the criterion defining the mechanical stability, one expects the elastic constant, C_{44} to be positive for a given material [27]. Although the calculated C_{44} of the tetragonal CuI satisfies this criterion, it is close to zero suggesting that the tetragonal phase may not be very stable.
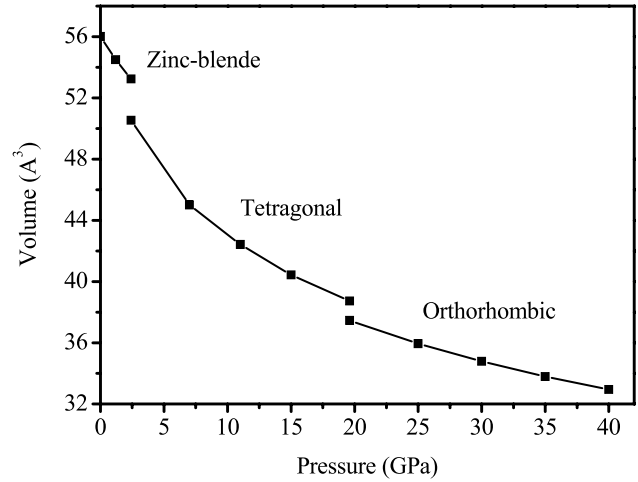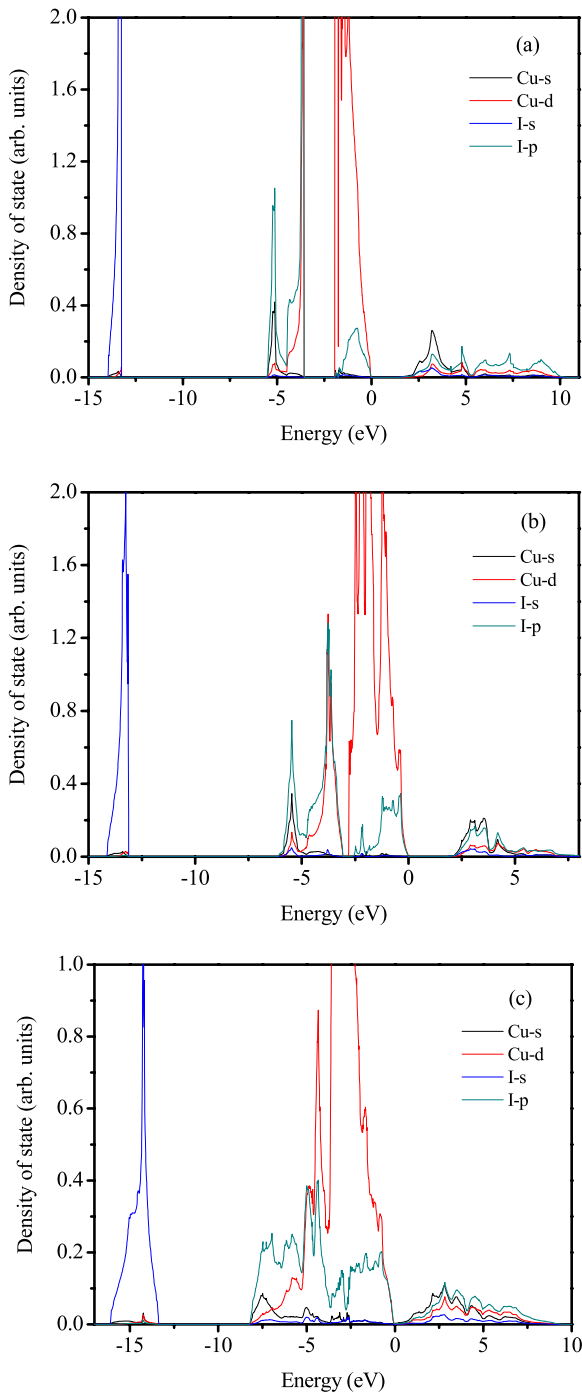
Figure 5. The projected density of states of CuI: (a) zinc-blende, (b) tetragonal, and (c) orthorhombic. Zero is aligned to the top of the valence band.
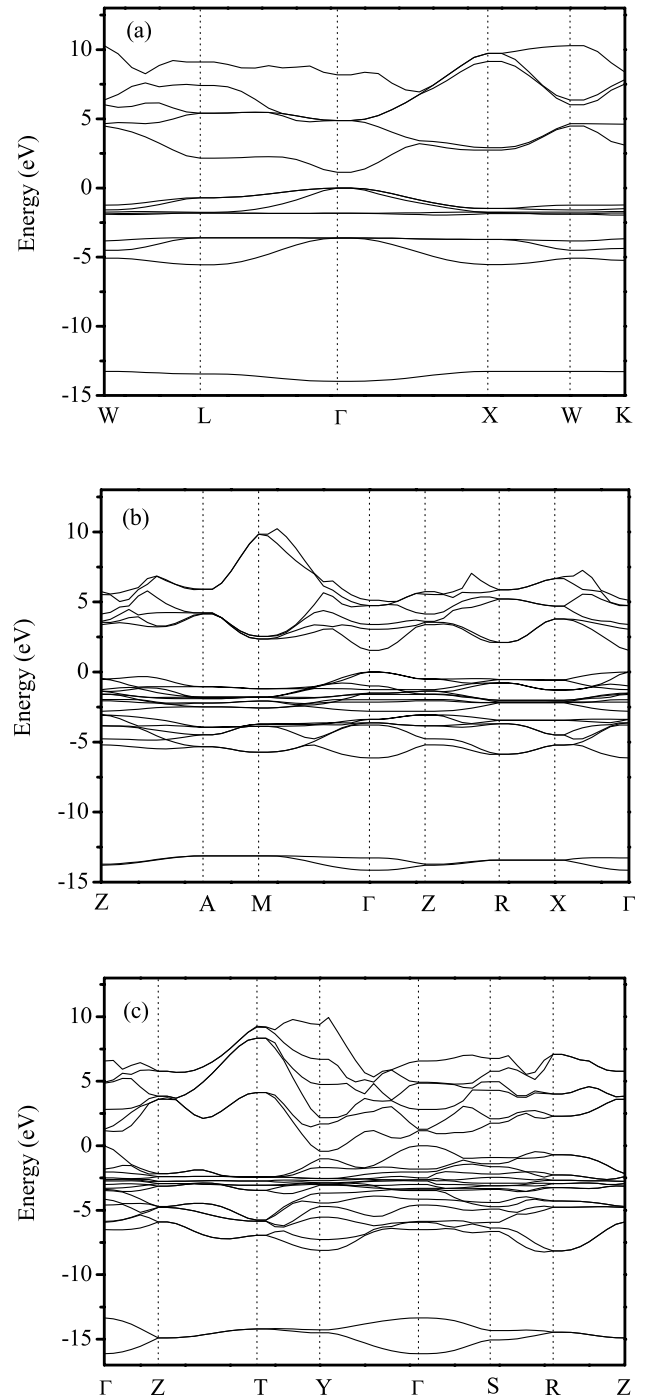

Figure 6. The calculated band structures of CuI: (a) zinc-blende, (b) tetragonal, and (c) orthorhombic. Zero is set as the top of the valence band.

materials. Nevertheless distinct features in the band structures of the polymorphs are clearly demonstrated by the method employed here.

The calculated effective mass of electron and light and heavy hole at Γ for polymorphs of CuI are also listed in table 3. We have fitted the energy dispersion of VBM (CBM) to a parabolic function in the vicinity of Γ to calculate the hole (electron) effective mass. For the zinc-blende phase, the average effective masses of electron and heavy hole are

in excellent agreement with the corresponding experimental values [28]. For example, the calculated value of the electron effective mass is 0.33 as compared to the corresponding experimental value of 0.34. Note that the calculated values of the electron or hole effective mass mimic the anisotropy of the Brillouin zone, and are comparable to those associated with most of the ionic materials, suggesting that the electronic conduction in CuI is possible only if the electrons can be

Table 2. Elastic properties of CuI in the zinc-blende, tetragonal and orthorhombic phases. Voigt, Reuss and Hill notation are labeled as V, R and H.

	Zinc-blende		Tetragonal		Orthorhombic	
	This work	Expt [24, 25]	This work	Expt [8]	This work	Expt [22]
Elastic constant (GPa)						
C_{11}	50.4	45.1	78.8		137.6	
C_{12}	33.5	30.7	24.7		34.2	
C_{13}			40.3		74.0	
C_{22}					185.8	
C_{23}					90.4	
C_{33}			56.2		129.3	
C_{44}	20.4	18.5	0.6		19.6	
C_{55}					73.3	
C_{66}			6.4		58.4	
Bulk modulus (GPa)						
K_V	39.1	35.5	47.2	50.0	94.4	115
K_R	39.1		47.0		92.1	
K_H	39.1		47.1		93.3	
Shear modulus (GPa)						
G_V	15.6		9.9		47.2	
G_R	13.0		2.3		34.3	
G_H	14.3		6.1		40.7	
Elastic modulus (GPa)						
B_X	117.4		161.5		197.2	
B_Y					314.6	
B_Z			112.4		383.0	
Debye temperature (K)	175.0	165.0	115.8		294.2	

Table 3. Electronic properties of the zinc-blende, tetragonal and orthorhombic phases of CuI.

	Zinc-blende	Tetragonal	Orthorhombic
Direct gap (eV)	1.13	1.54	Metallic
I 5s band width (eV)	0.72	1.02	2.78
I 5p band width (eV)	5.54	6.13	8.24
Separation I 5s–I 5p (eV)	7.72	7.0	5.12
Effective mass (m_e)			
Electron	Γ–L: 0.34	Γ–Z: 0.41	
	Γ–X: 0.33	Γ–M: 0.36	
Light hole	Γ–L: 0.38	Γ–M: 0.55	
	Γ–X: 0.50		
Heavy hole	Γ–L: 1.14	Γ–Z: 1.45	
	Γ–X: 1.54	Γ–M: 1.22	

promoted to the conduction band by overcoming the relatively large band gap.

3.5. Optical properties

Electronic structure calculations can also predict the nature and location of the interband transitions in a crystal which will assist the experimentalists in identifying the peaks in the optical spectra obtained by either reflectance or photoelectron spectroscopy. The transition intensities are determined by the overlap of the wave function of initial and final state or transition matrix elements according to equation (2). According to the selection rules, the transitions of p → s, p → d and d → p are allowed. The transition associated with p → p, d → s and d → d are forbidden.

Figure 7 depicts the average dielectric function of CuI in the zinc-blende, tetragonal and orthorhombic phases. In the zinc-blende phase, the peaks in the imaginary part of dielectric

function at 4.43, 6.00 and 6.86 eV are associated with the interband transitions of X_{3v}–X_{1c}, W_{2v}–W_{1c} and K_{6v}–K_{1c}, respectively. The imaginary part of dielectric function of zinc-blende at 2.4 GPa shows a blue shift compared to that at the ambient pressure (not presented). It is consistent to the results reported for ZnO [29]. In the tetragonal phase, the peaks at 3.90, 4.30, 5.35, 5.87 and 6.60 eV are contributed from the transitions of Γ_{3v}–Γ_{2c}, M_{7v}–M_{1c}, A_{1v}–A_{3c}, X_{5v}–X_{1c} and Z_{11v}–Z_{2c}, respectively. Compared to zinc-blende, the low energy absorption band at 1.86 eV disappears due to the augment of band gap in the tetragonal CuI. For the orthorhombic phase, the interband transitions of Γ_{8v}–Γ_{2c}, S_{7v}–S_{1c} and Z_{9v}–Z_{3c} result in the peaks in the imaginary part of dielectric function at 4.26, 4.80 and 6.95 eV, respectively.

Table 4 lists the calculated dielectric constants and refractive indices of the CuI polymorphs. For the zinc-blende phase, calculated dielectric constant is 6.52 which is in excellent agreement with experimental value of 6.5 [24]. Note

Table 4. Dielectric constants and refractive indices of polymorphs of CuI.

	Zinc-blende	Tetragonal	Orthorhombic
Dielectric constant			
This work	6.52	6.63	12.32
Experiment [24]	6.5		
Previous study-theory [12]	4.2		
Refractive index			
This work	2.55	2.57	3.51
Previous study-theory [12]	2.05		
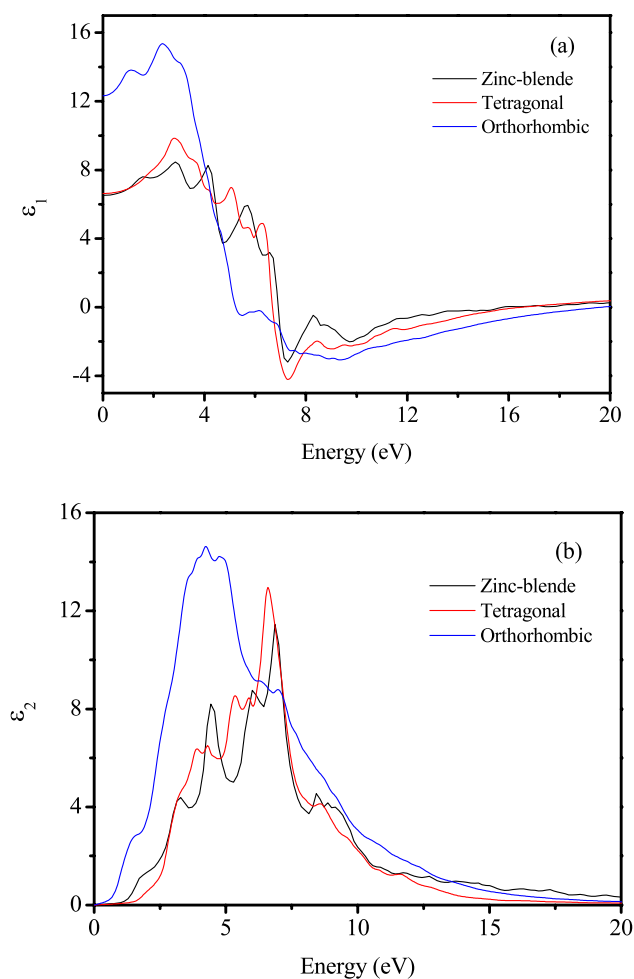
Figure 7. The calculated average (a) real part and (b) imaginary part of dielectric function of polymorphs of CuI.

4. Summary

The results of a comprehensive investigation of the polymorphs of CuI are reported. The calculated structural, elastic and optical properties of the zinc-blende CuI are in excellent agreement with the corresponding experimental values. The zinc-blende and tetragonal CuI are direct gap semiconductors and their optical properties are similar to each other. The orthorhombic CuI becomes metallic under high pressure. The valence band is almost flat indicating a rather large effective mass for holes for the polymorphs of CuI considered.

It has been suggested that CuI makes a transition to the rhombohedral phase for pressures <1.4 GPa [8–10]. This is in contrast to what has been predicted by our calculations based on density functional theory. We find a negative value of B_Z for the rhombohedral phase suggesting its mechanical instability. We also note that the rhombohedral phase does not exist for the other I–VII compounds such as AgI and CuBr [30]. A new experimental study is therefore warranted to confirm our predictions for the high-pressure polymorphs of CuI.

Acknowledgments

that the linear response of the system to an electromagnetic radiation is described by the dielectric function, which is directly related to the polarizability of the crystal. The polarizability, which represents the deformability of the electronic distribution, is to be connected with the shape of the valence charge density. Thus, a similarity in dielectric as well as optical properties between the zinc-blende and tetragonal phases is expected, as was predicted in the present study. A relatively large dielectric constant of CuI in the high-pressure orthogonal phase is likely to be due to the denser packing of ions and higher coordination number in the lattice.

References

[1] Adipranoto D S, Shikanai F, Yonemura M, Mori K, Park J G, Itoh K and Kamiyama T 2009 *Solid State Ion.* **180** 492–6
[2] Lewonczuk S, Ringeissen J, Beaurepaire E and Khan M A 1994 *Phys. Rev.* B **49** 2344–50
[3] Ichida H, Kanematsu Y, Shimomura T, Mizoguchi K, Kim D and Nakayama M 2005 *Phys. Rev.* B **72** 045210
[4] Perera V P S and Tennakone K 2003 *Sol. Energy Mater. Sol. Cells* **79** 249–55
[5] Derenzoa S E, Weber M J and Klintenberg M K 2002 *Nucl. Instrum Methods Phys. Res.* A **486** 214–9
[6] Gao P, Gu M, Liu X, Liu B and Huang S 2009 *Appl. Phys. Lett.* **95** 221904

[7] Sekkal W, Zaoui A, Laref A, Certier M and Aourag H 2000 *J. Phys.: Condens. Matter* **12** 6173–82

[8] Hull S and Keen D A 1994 *Phys. Rev. B* **50** 5868–85

[9] Blacha A, Christensen N E and Cardona M 1986 *Phys. Rev. B* **33** 2413–21

[10] Ves S, Glotzel D, Cardona M and Overhof H 1981 *Phys. Rev. B* **24** 3073–85

[11] Hernandez-Cocoletzi H, Cocoletzi G H, Rivas-Silva J F, Flores A and Takeuchi N 2009 *J. Nano Res.* **5** 25–30

[12] Amrani B, Benmessabih T, Tahiri M, Chiboub I, Hiadsi S and Hamdache F 2006 *Physica* B **381** 179–86

[13] Singh R K and Gupta D C 1989 *Phys. Rev. B* **40** 11278–83

[14] Yuce G, Çolakolu K, Deligoz E and Çiftci Y O 2007 *AIP Conf. Proc.* **899** 674

[15] Groh D, Pandey R, Sahariah M B, Amzallag E, Baraille I and Rerat M 2009 *J. Phys. Chem. Solids* **70** 789–95

[16] Kresse G and Furthmuller J 1996 *Phys. Rev. B* **54** 11169–86

[17] Kresse G and Joubert D 1999 *Phys. Rev. B* **59** 1758–75

[18] Perdew J P, Burke K and Ernzerhof M 1996 *Phys. Rev. Lett.* **77** 3865–8

[19] Groh D, Slough W J, Pandey R, Karna S P and Dandekar D 2011 *Phys. Rev. B* **83** 115122

[20] Gajdos M, Hummer K, Kresse G, Furthmüller J and Bechstedt F 2006 *Phys. Rev. B* **73** 045112

[21] Sampath S K, Kanhere D G and Pandey R 1999 *J. Phys.: Condens. Matter* **11** 3635–44

[22] Hofmann M, Hull S and Keen D A 1995 *Phys. Rev. B* **51** 12022–5

[23] Baghmar D, Gaur N K and Gupta D C 2010 *Physica* B **405** 133–9

[24] Hanson R C, Hallberg J R and Schwab C 1972 *Appl. Phys. Lett.* **21** 490–2

[25] Vardeny Z, Gilat G and Moses D 1978 *Phys. Rev. B* **18** 4487–96

[26] Ravindran P, Fast L, Korzhavyi P A, Johansson B and Eriksson O 1988 *J. Appl. Phys.* **84** 4891–904

[27] Wu Z, Zhao E, Xiang H, Hao X, Liu X and Meng J 2007 *Phys. Rev. B* **76** 054115

[28] Wang J, Li J and Li S 2011 *J. Appl. Phys.* **110** 054907

[29] Sun J, Wang H, He J and Tian Y 2005 *Phys. Rev. B* **71** 125132

[30] Keen D A and Hull S 1993 *J. Phys.: Condens. Matter* **5** 23–32